Article:
Kehler, M., Zhou, K., Kemas, A.M. et al. (2025) Organocatalytic switches of DNA glycosylase OGG1 catalyze a highly efficient AP-lyase function. Chemistry – A European Journal, 31 (33). e202500382. ISSN: 0947-6539

https://doi.org/10.1002/chem.202500382

Chemistry–A European Journal

Research Article
doi.org/10.1002/chem.202500382

Chemistry Europe
European Chemical Societies Publishing

www.chemeurj.org

Organocatalytic Switches of DNA Glycosylase OGG1 Catalyze a Highly Efficient AP-Lyase Function

Mario Kehler,[a] Kaixin Zhou,[a] Aurino M. Kemas,[b, c] Alicia del Prado,[d] Emma Scaletti Hutchinson,[e] Elinor Hesslefors Nairn,[a] Marek Varga,[a, f] Yvonne Plattner,[b, c] Yi Zhong,[b, c] Oryn Purewal-Sidhu,[a] James Haslam,[a] Elisée Wiita,[a] Heather Gildie,[a] Karolina Singerova,[a] Zuzanna Szaruga,[a] Ingrid Almlöf,[a] Femke M. Hormann,[a] Kang-Cheng Liu,[c, g] Olov Wallner,[a] Florian Ortis,[a] Evert J. Homan,[a] Opher Gileadi,[c, g] Sean G. Rudd,[a] Pål Stenmark,[e] Miguel de Vega,[d] Thomas Helleday,[a, h] Nicholas D. D'Arcy-Evans,[a] Volker M. Lauschke,[b, c, i, j, k] and Maurice Michel*[a, c]

8-oxoGuanine DNA glycosylase 1 (OGG1) is the first known target of organocatalytic switches (ORCAs), which rewrite the biochemical function of the enzyme through redirection of its preferred substrate from 8-oxoG to AP sites. Previously, different ORCA chemotypes were shown to enhance the operational pH window for OGG1, possibly through direct involvement in proton transfer events during DNA strand cleavage. Accordingly, compound pK_a is a crucial and necessary consideration for the identification and application of future OGG1 ORCAs. Here, we identify a minimal structure of organocatalytic switches–4-anilino pyridines and 6-anilino pyrimidines–which are dimethyl-amino-pyridine (DMAP)-type Brønsted bases binding the active site of OGG1. Systematic interrogation of compound basicity through modulation of electron-withdrawing (EWG) and electron-donating (EDG) substituents reveals that a pK_a less or equal to the assay pH is a viable parameter for prediction of compound activity. The lead structure (AC_{50} 13 nM, pK_a 7.0) was then identified as a potent scaffold from a screen in a patient-derived 3D model of metabolic dysfunction-associated steatohepatitis (MASH), where it reduced hepatic fibrosis by 35%. Collectively, these findings deepen the knowledge of this novel modulator class, with important implications for future enzyme targets and probe development.

[a] *M. Kehler, K. Zhou, E. H. Nairn, M. Varga, O. Purewal-Sidhu, J. Haslam, E. Wiita, H. Gildie, K. Singerova, Z. Szaruga, I. Almlöf, F. M. Hormann, O. Wallner, F. Ortis, E. J. Homan, S. G. Rudd, T. Helleday, N. D. D'Arcy-Evans, M. Michel*
Science for Life Laboratory, Department of Oncology-Pathology, Karolinska Institutet, Stockholm, Sweden
E-mail: maurice.michel@ki.se

[b] *A. M. Kemas, Y. Plattner, Y. Zhong, V. M. Lauschke*
Department of Physiology and Pharmacology, Karolinska Institutet, Stockholm, Sweden

[c] *A. M. Kemas, Y. Plattner, Y. Zhong, K.-C. Liu, O. Gileadi, V. M. Lauschke, M. Michel*
Center for Molecular Medicine, Karolinska Institutet and Karolinska Hospital, Stockholm, Sweden

[d] *A. del Prado, M. de Vega*
Centro de Biología Molecular 'Severo Ochoa' (CSIC-UAM), Nicolás Cabrera 1, Cantoblanco, Madrid, Spain

[e] *E. S. Hutchinson, P. Stenmark*
Department of Biochemistry and Biophysics, Stockholm University, Stockholm, Sweden

[f] *M. Varga*
EaStCHEM, School of Chemistry, University of St. Andrews, St. Andrews, UK

[g] *K.-C. Liu, O. Gileadi*
Structural Genomics Consortium, Department of Medicine Solna, Karolinska Institutet, Stockholm, Sweden

[h] *T. Helleday*
Sheffield Cancer Centre, Department of Oncology and Metabolism, University of Sheffield, Sheffield, UK

[i] *V. M. Lauschke*
Dr. Margarete Fischer-Bosch Institute of Clinical Pharmacology (IKP), Stuttgart, Germany

[j] *V. M. Lauschke*
University of Tübingen, Tübingen, Germany

[k] *V. M. Lauschke*
Department of Pharmacy, the Second Xiangya Hospital, Central South University, Changsha, China

Mario Kehler, Kaixin Zhou, and Nicholas D. D'Arcy-Evans are contributed equally to this work.

Supporting information for this article is available on the WWW under https://doi.org/10.1002/chem.202500382

1. Introduction

Among the most prevalent oxidative DNA lesions is 8-oxoguanine (8-oxoG), formed from the reaction of the guanine nucleobase with ubiquitous reactive oxygen species (ROS), generated from ordinary cellular metabolism. At the outset of the repair process, 8-oxoguanine DNA glycosylase 1 (OGG1) recognizes, binds to, and excises 8-oxoG from the DNA strand, generating an apurinic site (AP site), which initially remains tethered to OGG1 through a reversibly formed Schiff base. Release of OGG1 requires the onset of downstream enzyme apurinic/apyrimidinic endonuclease 1 (APE1), which performs an incision of the phosphate ester along the DNA strand. OGG1 itself may meagerly replicate this behavior through a β-elimination process from the tethered Schiff base, but this is slow and inefficient in vitro and without relevance in a cellular setting. Although often referred to as bifunctional, this renders OGG1 a de facto monofunctional glycosylase with cleavage of the Schiff base as the rate-determining step for the initiation of the ensuing base excision repair cycle.[1]

Notably, elevated levels of OGG1 and subsequent activity have shown promising potential for the treatment of numerous diseases and senescence. For example, boosting OGG1 concentration can protect against neurodegeneration, such as in Alzheimer's disease, by controlling the levels of 8-oxoG in the brain.[2,3] Similarly, transgenic mice with increased mitochondrial OGG1 levels are shielded from weight gain and obesity in high-fat diets.[4,5] Therefore, improving repair of oxidative DNA damage is an auspicious strategy for treatment or prevention of diseases linked to high oxidative stress.[6]

Next to its role in DNA repair, OGG1 influences transcriptional processes through recognition and binding of 8-oxoG in gene promoter regions. It has been established that the enzyme acts here as a transcription co-activator of NF-κB-mediated pro-inflammatory signaling.[7] Along these lines, metabolic dysfunction-associated steatohepatitis (MASH) is an example of a disorder characterized by secretion of extensive amounts of pro-inflammatory cytokines. Besides inflammation, oxidative stress is an important contributor to disease progression by causing stellate cell activation, fibrogenesis, and hepatic scarring. Furthermore, redox imbalance can raise DNA damage levels via oxidative pathways, and indeed, DNA damage response (DDR) can result in pathological polyploidization, thereby linking MASH to hepatocellular carcinoma.[8]

Functional enhancement of OGG1 activity has recently been achieved through the development of small molecules that promote the capacity for β-elimination through recognition of the intermediate state resulting from 8-oxoG excision.[9] Here, the affinity to this Schiff base-DNA-OGG1 conjugate locks the small molecule structure into position within the active site, facilitating abstraction of the acidic α-proton from the activated Schiff base by means of the compound's character as a Brønsted base. This triggers a strand cleavage event in the form of accelerated β-elimination, traditionally termed β-lyase activity. OGG1 and the small molecule are then released from the product and can enter a new catalytic cycle of excision and incision.

In cells, these compounds transform OGG1 function from a DNA glycosylase into an AP-lyase, effectively slowing 8-oxoG excision and instead enhancing the repair of multisource and more abundant AP sites. Due to these properties and the modified substrate preference they induce, small molecules in this class are termed organocatalytic switches, or ORCAs.[10,11] Indeed, applying OGG1 ORCAs in a patient-derived MASH model, we previously observed reduced collagen I excretion, DNA damage, and inflammation, as well as increased hepatocyte regeneration, reversing most of the hallmarks of liver fibrosis.[12] Similarly, we previously showed that treatment of cells under high oxidative stress with an ORCA resulted in an enhanced rate of DNA repair in the telomeric regions, highlighting the potential of these compounds to combat multiple hallmarks of aging.[13]

However, as a relatively new modulator class, key properties of ORCAs remain understudied. Besides the required selectivity between apo- and Schiff base-bound enzyme, the role of ORCAs as chemical bases is less well understood. Following the logic of elimination reactions, it has been shown recently that nitrogen base properties appear to guide the activity of the entire catalytic system.[10] As a descriptor of proton transfer reactions, pK_a is therefore uniquely suited to monitor compound activity. Since the dissociation constant describes the degree of protonation at a given pH, intuitively, the pK_a of an ORCA should be close to physiological pH to ensure a sufficiently large active mole fraction for catalysis. Despite this, the basic residues required for phosphate backbone binding mean that the local pH of the active site microenvironment of DNA-binding proteins is more difficult to estimate and is likely elevated.[14]

Still, the limiting factors in thoroughly investigating the role of compound pK_a are as follows: (1) the number of possibly active basic nitrogen atoms in currently known OGG1-ORCAs, (2) the limitation of available chemical space to install electron-withdrawing (EWG) or -donating groups (EDG) in these structures, and (3) a workflow that allows compound comparison across several conditions.[10,13]

Based on these considerations, we set out to identify a minimal structure of ORCAs targeting OGG1. Having previously optimized the active site affinity handle in the form of 3,4-dichloroaniline,[10,15] we synthesized single-ring heterocycles to generate 4-anilino pyridines and 6-anilino-pyrimidines as a minimal structure of OGG1 organocatalytic switches. After observing improved OGG1 activity, we generated a panel of matched pairs to systematically tune the pK_a of the involved nitrogen. Assessing each generated compound in four different pH environments revealed that the pK_a of the catalytically active nitrogen can be used as a stop-go strategy to design highly potent OGG1 ORCAs within the tolerated substitution pattern. In addition, we orthogonally confirmed that OGG1 ORCAs catalyze β-elimination at AP sites. Outstanding compounds were active below protein concentration, fulfilling the definition of catalysts. We further confirmed active site binding by assessing OGG1 mutant enzymes and obtained a co-crystal structure of an ORCA and OGG1. Using these compounds in a previously developed patient-derived screening model of MASH, we observed that this improved series outperformed tool compound TH10785 in resolving the fibrotic

organoid state. This study reveals valuable insights in the rational design of analogues of this novel compound class and informs future campaigns for the identification of chemical probes and drugs for OGG1 and related targets.

2. Results

2.1. 4-Anilino-pyridine and 6-Anilino-pyrimidine are Minimal Structures of Organocatalytic Switches

Previously, we investigated the binding of small molecule inhibitors at the deep catalytic pocket of OGG1, and furthermore, optimized aniline substituents as the preferred scaffold of organocatalytic switches (Table 1).[10,15] While evaluating nucleobase structures as the modified core, Hank et al. synthesized a number of purine derivatives (**a–c**) and a first pyrimidine analogue (**d**). Here, to potentially identify a minimal structure of organocatalytic switches, we started by combining small six-membered heterocycles with the preferred 3,4-dichloroaniline affinity handle (**1–6**, Table 1). All compounds were tested for AC50[13] using a fluorophore-quencher-based enzyme activation assay and target engagement of OGG1 using Nano-DSF.[10,13,15] This initial investigation revealed that modulating the nucleobase pyrimidine character by removing hydroxy groups and one ring nitrogen boosted the activity of the compound in a stepwise manner. Compound **1** started to show an effect at 100 µM, and hydroxy-pyridine **2** exhibited a substantial improvement, with activity at low µM concentration. Removing all hydroxy groups, 6-anilino pyrimidine **3** and the corresponding 4-anilino-pyridine **4** resulted in an AC50 of 540 and 13 nM, respectively, improving the compound activity by over 10,000-fold compared to **1**. To confirm the apparent 1,4-relationship of the aniline substituent and active center nitrogen, we generated analogues **5** and **6**, which were inactive. Interestingly, the identification of **4** highlighted the combination of active site affinity and the previously reported Brønsted base character of the compound.[10] **4** resembles the commonly used organic base DMAP, appended with an active site affinity to OGG1, and is so far the smallest and simplest structure for robust activation of the weak incision capability of OGG1.

Table 1. Removing pyrimidine nucleobase character identifies the smallest structures of organocatalytic switches.

#	Structure, R^1 = 3,4-Dichloroaniline	AC_{50} (CI95) [µM]	DSF [K]	pK_a
a	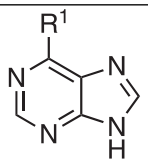	Inactive	n.d.	n.d.
b	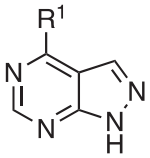	6.20 (4.70–8.20)	n.d.	n.d.
c	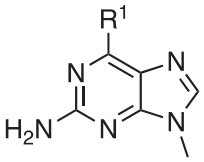	Inactive	n.d.	n.d.
d	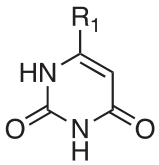	Inactive	n.d.	n.d.
1	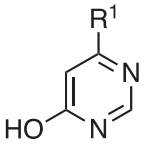	>100	1.5	9.2
2	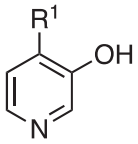	4.80 (3.60–6.60)	0.9	9.7
3	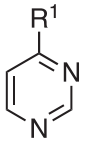	0.540 (0.250–1.200)	0.1	4.2
4	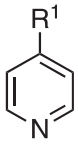	0.013 (0.010–0.016)	0.7	7.0
5	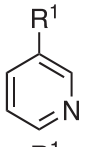	Inactive	1.0	n.d.
6	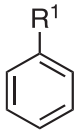	Inactive	1.5	n.d.

CI95, 95% confidence interval 95, n.d. not determined. Compounds with letters were reported earlier[10] and compounds with numbers were synthesized in this study.

2.2. Modulating Base Properties by Installing EDG and EWG

Having identified a minimal structure in pyridine **4**, we set out to produce analogues that modulate the electronics of the ring, and therefore the pK_a of the active nitrogen, through installation of various EWGs and EDGs at the 2- and 3-positions. The AC50 was then determined for the compounds, and protein stabilization was assessed using Nano-DSF.

Adding EDGs at the 2-position generally stabilized the protein, producing potent analogues with methyl (**7**), amino (**8**), and methoxy (**9**) substitution. Similarly, installation of small EWGs such as chloro (**10**) and trifluoromethyl (**12**) groups retained scaffold potency and stabilized OGG1. Interestingly, mesomerically withdrawing nitro (**11**) and cyano (**13**) groups

either showed reduced levels of stabilization or lowered compound activity up to 100-fold. The carboxylic acid and its derivatives (**14**–**16**) showed poorer levels of enzyme activation or complete inactivity and weak stabilization, suggesting inefficient active site binding. In turn, generating the 3-position matched pairs of amino (**17**) and cyano (**20**) groups saw an overall improvement of AC50, with nitro (**18**) as the least active compound. Fluorine analogue **19** was equally potent as lead compound **4** and is the second outstanding member of this chemical series. Finally, we generated the pyrimidine matched pairs (**22**,**23**) of amino- and chloro-substituted pyridines (**10**,**17**) and observed reduced activity compared to the pyridine series.

Scaffold A (pyridine)

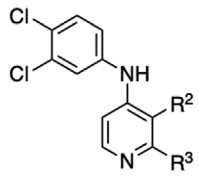

Scaffold B (pyrimidine):

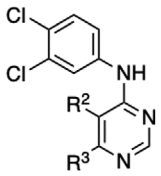

2.3. β-Elimination by OGG1 is Mediated by Selective Binding of 4 to the Active Site

To substantiate the mode of action of this series of OGG1 ORCAs, we independently confirmed the activity of **4** using SDS-PAGE. For both substrates, 8-oxoG and an AP site generated through *E.coli* uracil DNA glycosylase, an acceleration of the intrinsic β-elimination of OGG1 was observed in the presence of **4** (Figure 2A), generating a 3′-phospho α,β-unsaturated aldehyde (3′PUA). As established previously, TH10785 instigated a β,δ-elimination, also generating a 3′-phosphate (3′P).[13]

To determine the binding mode of **4**, we solved the X-ray co-crystal structure of mouse OGG1 complexed with the ligand to 2.64 Å resolution (Table S1). Unambiguous electron density for **4** was observed in the substrate binding pocket (Figure 1B). Due to more significant amenability to crystallization, mouse OGG1 was used for structural studies as it has an identical active site to human OGG1. **4** is positioned by H-bonds between the dichlorobenzene ring and the sidechain of Gln315, as well as an H-bond between the secondary amine linker and the backbone oxygen of Gly42. Furthermore, **4** engages in a π-stacking interaction with Phe319 and additional hydrophobic interactions involving Phe45, Phe144, Ile152, Ile155, Met257, and Pro266 (Figure 2B).

Comparison of the complexed **4**-mouse-OGG1 crystal with the previously reported structure of TH10785 (PDB ID: 7AYZ)[13] shows the good agreement between the two superimposed complexes with minor differences in Gly42 and Asp268, which are shifted slightly between the structures (Figure S1A/B). While the ligands occupy the same general area in the substrate binding pocket, their overall orientations differ considerably from one another (Figure 1SA). Specifically, TH10785 interacts through an H-bond with the sidechain of Asp268, which is not observed in the complex with **4**. Furthermore, residue Gln315 does not form any H-bonds with TH10785, as is observed for **4**. However, both ligands form an H-bond with the backbone oxygen of Gly42, and both are positioned by an important π-stacking interaction with Phe319, confirming our previously report and the SAR outlined above (Figure S1B).

The observations from the co-crystal structure confirming active site binding were corroborated by assessing the level of boosted activity upon treatment with **4** for the wild-type enzyme (wtOGG1) and OGG1 mutants: S326C, C253Y, F319A, and K249W. Improved β-lyase activity was observed for wtOGG1 and S326C, but no activation was observed for mutants containing active site permutations, further supporting proposed model of orthosteric binding of **4** (Figure 1C).

To further study the enzyme-compound complex, we performed studies in saturation kinetics using the substrates 8-oxoA and an AP site opposite cytosine (Figure 1D–F). We observed that upon treatment with **4**, OGG1 addressed AP sites much more efficiently than 8-oxoA, with a 40-fold rate enhancement for the former and an 8-fold rate enhancement for the latter, compared to untreated OGG1. Notably, for both substrates the acceleration effect was measurable at compound concentrations below protein concentration at 10 nM, demonstrating catalytic behavior of the small molecule.

We wondered whether this rate enhancement was general for OGG1-mediated AP site cleavage and therefore determined the slope of the reaction at AP sites opposite the three remaining canonical nucleobases, as well as in single-stranded DNA. At a concentration of 125 nM, the presence of **4** facilitated enhanced cleavage of AP sites opposite adenine (38.7%), guanine (40.5%), and thymine (27.3%), compared to cytosine. On the contrary, OGG1 remained inactive in single-stranded DNA (Table S2). These results demonstrate that the presence of **4** imparts the complete biochemical profile of AP-lyase capability to OGG1 for double-stranded DNA substrates. Furthermore, the rate enhancements observed for the AP sites were all higher than the combined rate of base excision and AP site incision for 8-oxoA:C (17.5%), suggesting that the rate-limiting step in the canonical biochemical cascade has shifted from AP-lyase DNA binding to excision of the oxidized nucleobase.

Last, we determined the selectivity of compound **4** for OGG1. Screened on an in-house panel of DNA glycosylases and NUDIX family members, no effect was observed, confirming selectivity for OGG1 over other proteins binding DNA and nucleotides (Table S3).

2.4. pK_a of Minimalist Organocatalytic Switches Control Enzymatic Activity in Distinct pH Environments

We then sought to determine whether the pK_a of the pyridine and pyrimidine structures would influence enzymatic activity. Using the Schrödinger Maestro module Epik,[16] we calculated the pK_a for each compound (Tables 1 and 2) and the slope of OGG1 activity on 8-oxoA was measured in four different pH environments: 6.7, 7.1, 7.4, and 8.0. We then plotted the compounds as a function of pK_a and their resulting slope as a function of activation of strand break generation at each pH (Figure 2).

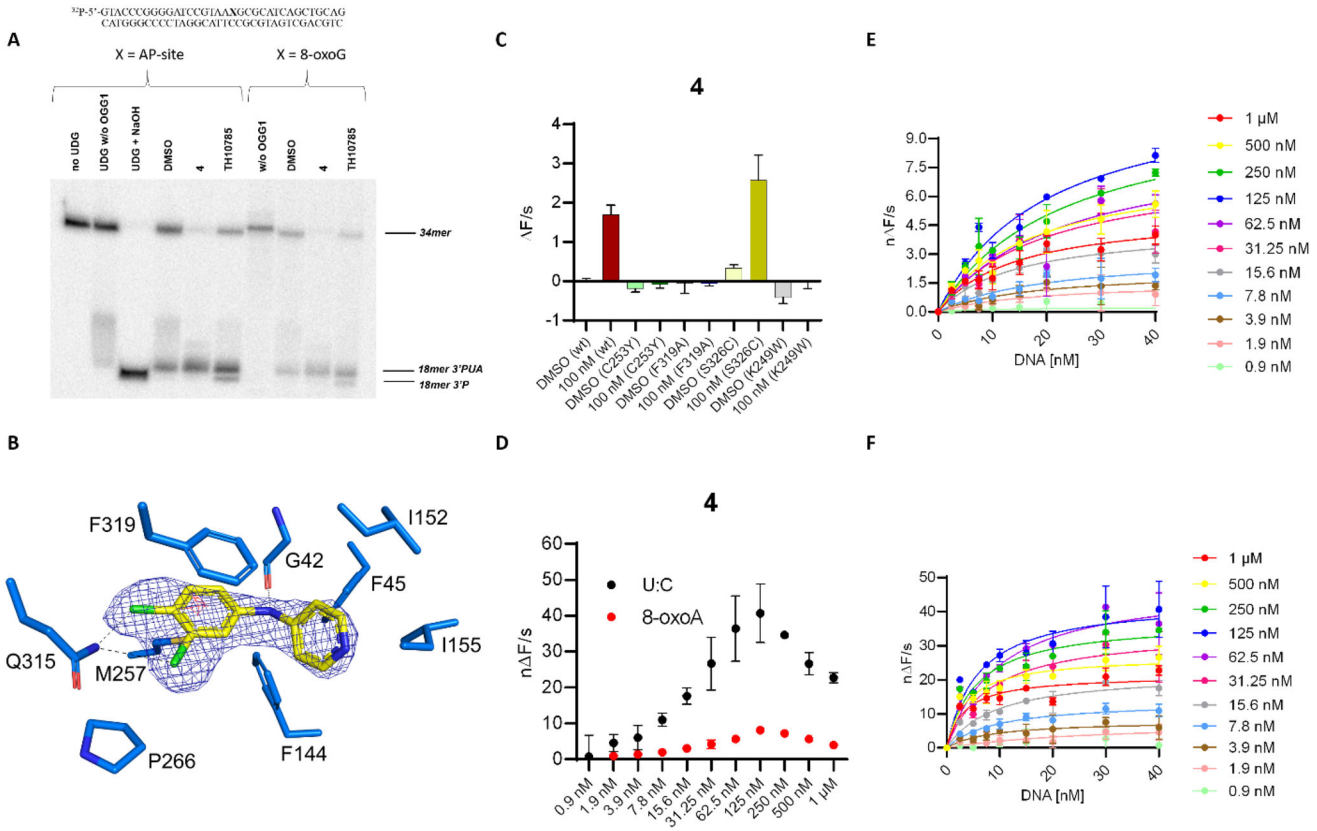

Figure 1. Organocatalytic switch 4 acts from within the active site and establishes β-elimination at concentrations lower than that of OGG1. (A) PAGE using ^{32}P-labeled DNA oligos indicates a β-elimination catalyzed by **4** in interplay with OGG1 on both AP-site and 8-oxoG substrate, oligo sequence as indicated; UDG, NaOH, DMSO, and TH10785 serve as controls. (B) The recognition of **4** by mouse OGG1: amino acids contributing to ligand binding are depicted as sticks; C atoms are colored blue, O atoms red, N atoms dark blue, and S atoms gold. **4** is shown as a stick model; C atoms colored yellow, N atoms coloured dark blue, and Cl atoms coloured green. Hydrogen bond interactions are shown as dashed lines. The 2Fo−Fc electron density map around **4** is contoured at 1.0 σ (blue), and the Fo−Fc electron density maps are contoured at −3.5 σ (red) and + 3.5 σ (green). Figure produced with PyMOL (v.2.3.3, Schrödinger). (C) Activity of OGG1 mutants indicates active site binding, the slope of the reaction was measured on 8-oxoA substrate in the presence of DMSO or 100 nM organocatalytic switch **4**, wild-type (wt) OGG1, C253Y, F319A, and K249W at 10 nM; S326C at 50 nM; substrate at 10 nM, $\Delta F/s$ change of fluorescence per second; (D–F) Saturation kinetics reveal boosted incision activity at concentrations lower than that of OGG1, saturation kinetics with **4** were performed at 40 nM of both DNA substrates (40 nM) (D) and for all indicated concentrations separately on 8-oxoA (E) and AP-sites (F); n$\Delta F/s$ change of fluorescence per second normalized for DMSO, AP-sites were generated from U:C using UNG2. 40 nM conditions in (E) and (F) are identical in (D).

In accordance with literature,[10,13] OGG1 alone exhibited inactivity (pH 6.7) and weak activity (pH 7.5) at all other conditions. With APE1 present, the activity slope was increased for all conditions, indicating that OGG1 is outside of functional pH for AP site incision while retaining glycosylase activity. Consequently, ten compounds demonstrated activation of OGG1 at a pH of 6.7. Compound **10** demonstrated the highest reactivity with the largest activity slope at 3.4 FU/s, achieved at 3.125 µM. Interestingly, for those compounds that appear active at pH 6.7, the majority have a low pK_a with values in the range of 0.84 (**23**) to 5.27 (**9**). Whereby, for those compounds with a pK_a greater than or equal to assay pH (6.7), only entry **7** and entry **8** showed activity with pK_a values of 8.23 and 8.10, respectively. Notably, entry **7** was an equally potent compound to **10** at pH 6.7 with a slope of 3.4 FU/s.

At pH 7.1, the APE1-coupled condition exhibited a maximum slope at this pH (3.9 FU/s) with an increased reaction rate, yet four organocatalytic switches activated OGG1 beyond APE1. Of these, three compounds–entries **10**, **18**, and **3**–had a pK_a between 2.98 and 4.21, while entry **7** remained highly active. The two most activating compounds at pH 7.1 (entries **3** and **18**) led to a >1.6-fold increase in slope relative to the APE1 condition, with slopes of 6.3 and 6.4 FU/s, respectively. Both compounds achieve a maximum slope at this pH compared to all other pH conditions. Additionally, entry **18** at 25 µM has led to a 39-fold increase in rate of reaction compared to OGG1 alone at the same pH (0.16 FU/s). More broadly, at least one concentration of 18 out of 23 organocatalytic switches led to an enhancement in slope at this pH relative to OGG1 alone. Overall, the greatest activity enhancement has been observed in going from pH 6.7 to 7.1, in which the compounds are with a pK_a at or below assay pH.

At pH 7.5, the results indicated that APE1 was still highly efficient (3.1 FU/s) and OGG1 alone was performing its rudimentary bifunctionality at a maximum rate (0.33 FU/s). As before, the most potent compounds had a lower pK_a, and this time closer to the assay pH. Compounds that saw their maximum slope at pH 7.1 exhibited a decrease in slope at pH 7.5, such as entries **16** (3.8 FU/s to 2.8 FU/s) and **3** (6.3 FU/s to 2.3 FU/s). Meanwhile, compounds with slightly higher pK_a continued to enhance OGG1 activity against AP sites at a higher, and apparently optimal pH

Research Article
doi.org/10.1002/chem.202500382
Chemistry Europe
European Chemical Societies Publishing

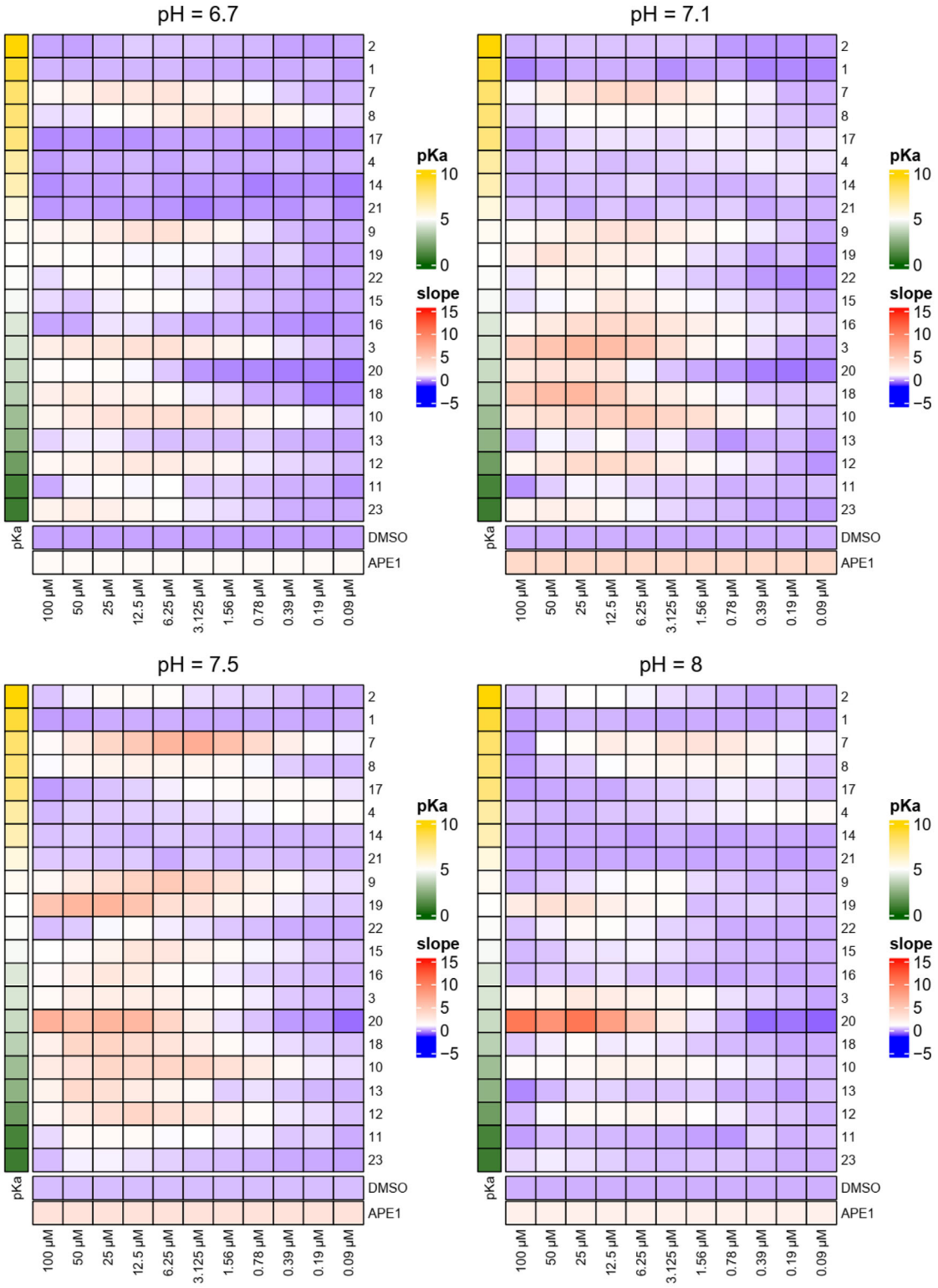

Figure 2. Modulation of OGG1 biochemistry across pH is dominated by compound pK_a: Compounds were tested in four different pH environments. OGG1 was incubated with different concentrations, and v_o was measured for all conditions in $\Delta F/s$. As a control, OGG1 alone and OGG1 + APE1 were added. In the final plot, compounds are arranged according to their individual pyridine nitrogen pK_a (left, green to yellow) and compared to v_o (blue, via white to red) of each condition defined by pH and compound concentration. The average reaction slope was calculated for independent replicates, each in duplicate.

Table 2. Focused SAR for the modulation of nitrogen pK_a in a series of organocatalytic switches based on pyridine and pyrimidine.

#	Scaffold	R^2	R^3	AC_{50} (CI95) [μM]	DSF [K]	pK_a
7	A	—H	—Me	0.160 (0.130–0.190)	1.5	8.2
8	A	—H	$—NH_2$	0.080 (0.060–0.090)	1.5	8.1*
9	A	—H	—OMe	0.410 (0.250–0.670)	−1.8	5.3
10	A	—H	—Cl	0.200 (0.160–0.240)	1.4	3.08
11	A	—H	$—NO_2$	9.50 (6.10–14.6)	1.2	1.15
12	A	—H	$—CF_3$	0.440 (0.280–0.690)	2.4	1.9
13	A	—H	—CN	3.08 (1.87–5.09)	0.3	2.6
14	A	—H	—COOH	Inactive	0.7	6.7
15	A	—H	—COOMe	1.63 (1.37–1.92)	0.7	4.8
16	A	—H	$—CONH_2$	3.69 (3.03–4.48)	0.6	4.3
17	A	$—NH_2$	—H	0.100 (0.080–0.120)	1.1	7.9*
18	A	$—NO_2$	—H	1.09 (1.06–1.12)	0.8	3.6
19	A	—F	—H	0.010 (0.009–0.011)	0.9	5.009
20	A	—CN	—H	1.10 (1.10–1.20)	0.9	3.9
21	A	—COOH	—H	Inactive	0.7	5.7
22	B	$—NH_2$	—H	2.00 (1.30–3.00)	0.7	5.0
23	B	—H	—Cl	6.00 (4.50–7.90)	2.1	0.8

* The most basic nitrogen is amine. CI95 confidence interval 95.

7.5. The average pK_a of the three most potent compounds at pH 7.5 was 5.70 compared to an average pK_a of 3.58 for the three most potent compounds at pH 7.1. The largest slopes in this condition were achieved by entries **19**, **20**, and **7** at 6.6 FU/s, 6.7 FU/s, and 6.9 FU/s, respectively.

In the final assay condition, pH 8.0, OGG1 alone exhibited a very weak AP-lyase activity comparable to that seen at pH 7.1 (0.2 FU/s at pH 6.7; 0.2 FU/s at pH 8.0). Activity of APE1 also decreased relative to both pH 7.1 and 7.5, reaching a slope of 2.1 FU/s. Beyond these control conditions, all previously active compounds saw a considerable decrease in activity at the higher pH. The exception was compound **20**, whose ability as an organocatalytic switch appears only to improve as pH increases. It led to the single highest slope recorded in this study at 10.6 FU/s, yet at a relatively high concentration of 100 μM. This is a 62-fold improvement on the rate of OGG1 alone and a 5-fold increase in rate compared to the APE1-coupled condition. Even across pH, this slope is nearly 33 times greater than the fastest observed OGG1 activity against AP sites (pH 7.5) and almost three times faster than the quickest APE1-coupled activity (pH 7.1).

2.5. Chemical Tuning of OGG1 Modulators Enhances Antifibrotic Efficacy

To advance our findings toward therapeutic applications, we had previously identified that OGG1 modulation could exert antifibrotic effects in a patient-derived ex vivo model of metabolic dysfunction-associated steatohepatitis (MASH).[12] Among the tested molecules, TH10785 and **4** emerged as top candidates that significantly reduced pro-collagen I levels (Figure 3A). Here,

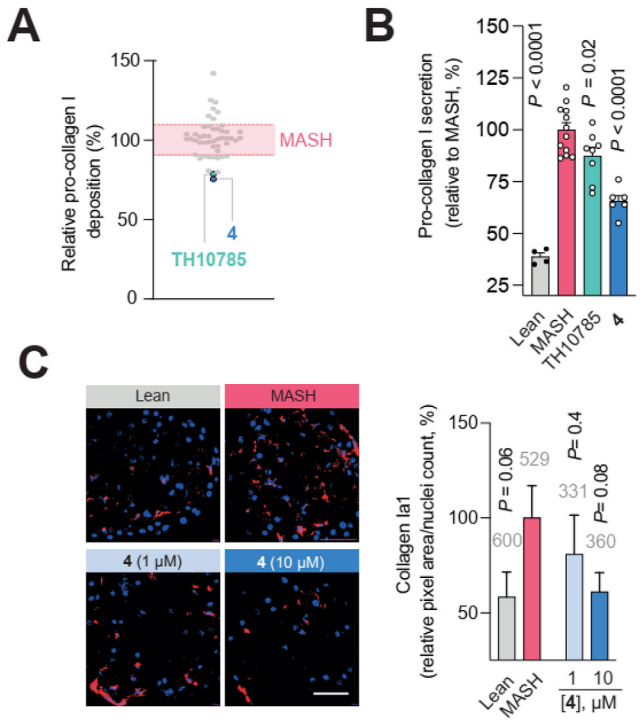

Figure 3. ORCA 4 exerts significant anti-fibrotic effects in a patient-derived 3D MASH model. (A) Previous screening results of anti-fibrotic compounds in a spheroid MASH model identified TH10785 and **4** as top candidates.[12] (B) Treatment with **4** (10 μM) significantly reduced pro-collagen I secretion in independent experiments. Note the improved efficacy compared to TH10785 (10 μM). n = 4–12 biological replicates. (C) Immunostaining of COL1A1 in cryo-sectioned MASH spheroids confirmed a dose-dependent reduction in collagen I expression after one week of exposure to compound **4**. Numbers in grey indicate the total number of cells analyzed. Scale bar = 50 μm. *P* values refer to the two-sided Student's *t*-test, comparing the treatment groups to MASH. Data are presented as mean ± s.e.m.

we sought to test whether the increased chemical understanding of original ORCA TH10785 yielded previously[10] and above would also result in enhanced biological activity of **4**. Indeed, treatment of MASH 3D cultures with **4** significantly reduced pro-collagen I secretion by 35% compared to untreated controls, which exceeded the efficacy of TH10785 (Figure 3B). These results were corroborated by COL1A1 immunostaining of cryo-sectioned spheroids, which revealed a dose-dependent reduction in collagen I deposition (Figure 3C).

3. Discussion

Organocatalytic switches are a novel, yet understudied, modality. As reagents, they partake in the biochemical reaction of the enzyme of interest, however, little is known about the properties necessary to monitor during compound optimization. ORCAs unite both active site affinity and a reactive center in one molecule,[11] properties that reveal two potential new parameters to be optimized during a medicinal chemistry campaign. First, while active site affinity is commonly optimized when designing competitive inhibitors, organocatalytic switches of OGG1 require

a selectivity for binding the Schiff-base-DNA-enzyme conjugate over merely blocking the active site of the enzyme. Second, the reactive center of an ORCA brings with it a nitrogen atom with suitable pK_a in an appropriate position for proton abstraction from the α-carbon of the Schiff base.

The comparably simple solution to the former challenge is the measurement of biochemical activity of OGG1 in the presence of an ORCA, which referred to as the AC50 in the literature.[10,13] The lower an AC50, the more active a compound is in the interplay with OGG1. Should the ORCA also have an affinity for the apoenzyme and thus exclude some of the substrate from conversion, selectivity might be impaired. Due to the connectivity between two enzymatic activities of OGG1, inactivity or inhibition is observed when the affinity is measurable as an IC50 and is close to the AC50–in other words, no AP lyase activity will be observed if no base excision has occurred prior to that. In contrast, a significant difference in the two values will lead to a bell-shaped activity curve, which was previously observed for TH10785 and other compounds.[10,13] The goal of an optimization is then the removal of affinity to OGG1 alone or an increased selectivity window between AC50 and competitive concentration. In the literature, a 30-fold difference is accepted to be selective within the protein family or for relevant closely related targets.[17] Due to the nature of the optimization problem of targeting the same protein in two different but interconnected activity states, it appears that a 30-fold selectivity is still too unspecific, and future research and the community need to thoroughly investigate and judge the challenge. However, we have successfully triaged the selectivity challenge for a number of compounds before with either no competition effect in the assessed concentration range up to 100 µM or sufficient, greater than 50-fold, selectivity.[10,13]

The second challenge was traditionally hampered by the presence of a larger number of nitrogen atoms within reported ORCAs. In addition, due to the complexity of the molecules on the one hand and the limited space for binding in the Schiff-base-DNA-enzyme conjugate on the other hand, handles to modulate nitrogen pK_a are challenging to identify. To address this, we first set out to identify a minimum structure of OGG1-ORCAs. Removing nucleobase character indeed led to the identification of very potent ORCAs of the 4-anilino-pyridine type (Table 1). While confirming a 1,4-relationship of active center nitrogen and aniline substituent, it also conveniently yielded a molecular series with only two positions available for immediate pK_a modulation. We then assembled a set of the smallest ORCA structures reflecting a breadth of nitrogen pK_a (0.8–8.2) and AC50 ranging over 1000-fold from 10 to10 nM (Table 2).

Anilino-pyridine **4** as the minimum structure was then further studied to assess the mode of action. A 32P-labeled DNA gel confirmed an increased β-elimination on both 8-oxoA and AP site substrates (Figure 1A). This agreed with the logic of an elimination reaction in organic chemistry, where a proficient chemical base induces a larger amount of E2-type eliminations. To corroborate the required vicinity of the chemical base, that is, ORCA, and substrate, we then assessed OGG1 mutants for their activity, confirming occlusion of the ligand by mutation of the active site, while mutants from outside the active site were boosted in their activity.[6] Furthermore, a co-crystal structure of OGG1 and **4** established that the 4-amino pyridine series indeed binds the active site of OGG1 (Figure 1B,C). Despite the co-crystal structure being resolved without the Schiff base conjugate, overlay with the previously obtained structure of TH10785 indicated an orientation of **4** within OGG1 suitable for catalysis.[9,13]

We then performed saturation kinetics using the system of **4** and OGG1. Given an excess of DNA substrates, each OGG1 copy would be required to undergo several cycles of substrate binding and Schiff-base incision. Indeed, titration of **4** then revealed that a stimulation of OGG1 (10 nM) on AP sites (40 nM) was already visible at 1.9 nM, indicating high affinity of the compound to the intermediate conjugate (Figure 1D,F). The corresponding rate for the substrate 8-oxoA was significantly lower but still increased compared to the DMSO control (Figure 1E). This confirmed that in the presence of compounds like **4**, resolving the AP sites is no longer the rate-determining step of OGG1 catalysis on 8-oxoA substrates. Future research needs to establish whether extrusion, recognition, excision, or a combination thereof is dominating the turnover rate of OGG1 in this specific scenario.[18,19]

In a next step, we assessed whether the range of pK_a installed in the derivatives of **4** indeed influenced activity in different pH environments. The data presented in Figure 2 provided the opportunity to identify an optimal pK_a range to aim for in the design of novel organocatalytic switches. Here, the pK_a range for all compounds that stimulated OGG1 beyond the APE1-coupled condition regardless of pH was 0.8 to 8.2. This is of course, a wide range and relatively unhelpful, however, narrowing the criteria down to the three most rate-enhancing compounds at each pH is more revealing. The average lowest pK_a for the three most potent compounds was 3.4 while the average highest pK_a for the three most potent compounds was 6.1. A pK_a range of 3.4 to 6.1 is narrow enough to be a helpful guideline, as it follows the principle demonstrated thus far: organocatalytic switches perform best at an assay pH that is similar to or higher than their pK_a and yet sufficient to accommodate an enzyme in near-optimal condition.

The data provided here offers a representative glimpse into the first challenge of ORCA optimization, mentioned earlier in the discussion. Many analogues indeed follow a bell-shaped curve (Figure 3) with high activity at lower concentrations and rising to a maximum level at intermediate concentration. Further increasing the concentration then reduced the observed acceleration effect again. This observation is important, since it reveals that ORCAs may benefit from assessment in a range of concentrations spanning from µM to nM concentrations, biochemical assays indicate such an activity profile. In addition, while **4** has a favorable pK_a and convinces with an extreme AC_{50} of 13 nM, other analogues of the series are far superior in their ability to induce β-elimination events. However, their reactivity profile follows that of a bell-shaped curve at higher concentrations reflecting a less selective behavior. The bell-shaped profile of **4** (Figure 1D) is significantly shifted toward concentrations at low nM with a selectivity for competition of above 50-fold, making it the most convincing member of the series.

To gain further insight into the potential of this detailed chemical tuning, we then screened members in a

preclinical patient-derived assays for MASH and fibrosis.[12] MASH is currently the leading cause of liver transplants with limited pharmacological treatment options.[20,21] DNA damage induced by reactive oxygen species is known to play a central role in disease progression due to its detrimental effects on cell cycle regulation and polyploidization of hepatocytes.[8] By showing that compound **4** resulted in a higher anti-fibrosis efficacy compared to TH10785, we demonstrated that chemical tuning can provide rationally designed candidate molecules with higher potency and more favorable pK_a.

Collectively, these findings inform strategies for designing organocatalytic enzyme modulators to target DNA repair pathways and may guide the development of drugs targeting oxidative damage-induced chronic diseases, including but not limited to MASH.

Author Contributions

Mario Kehler, Kaixin Zhou and Nicholas D. D'Arcy-Evans contributed equally. Synthetic chemistry: Mario Kehler, Heather Gildie, Marek Varga, Karolina Singerova, Zuzanna Szaruga, Oryn Purewal-Sidhu, Olov Wallner, Florian Ortis, Nicholas D. D'Arcy-Evans and Maurice Michel. Computational Workflow/Chemistry: Femke M. Hormann, Yi Zhong, Evert J. Homan, Nicholas D. D'Arcy-Evans, and Maurice Michel. Structural Biology: Emma Scaletti Hutchinson, PålStenmark. Biochemistry: Mario Kehler, Kaixin Zhou, James Haslam, Alicia del Prado, Elisée Wiita, Ingrid Almlöf, Miguel de Vega, and Maurice Michel. Pharmacology: Aurino M Kemas, Yvonne Plattner and Volker M Lausckke. Supervision: Olov Wallner, Opher Gileadi, Florian Ortis, Sean G. Rudd, Miguel de Vega, Pål Stenmark, Volker M Lauschke and Maurice Michel. Resources and Funding: Thomas Helleday, Miguel de Vega, Sean G. Rudd, Pål Stenmark, Volker M Lauschke and Maurice Michel. Concept: Nicholas D. D'Arcy-Evans, Volker M Lauschke and Maurice Michel. Writing and editing: Mario Kehler, Kaixin Zhou, Aurino M Kemas, Emma Scaletti Hutchinson, Nicholas D. D'Arcy-Evans, Volker M Lauschke, and Maurice Michel.

Acknowledgements

We are thankful to Athina Pliakou, Mari Kullman Magnusson, Therese Pham, Kristina Edfeldt, Pontus Pettersson, Ivan Vilotijevic, Michael Sundström, and Allan Watson for administrative support. We thank Per Artursson and his lab for providing hepatocytes used for this study. We thank the Department of Biochemistry and Biophysics of the Stockholm University for access to the NMR facility. We thank MAXIV Laboratory (Sweden, proposal MX20240089), and their beamline scientists from the BioMAX beamline for their support in data collection. This work was funded by the Åke-Olsson foundation for haematological research (2020–00306 MM), the Helleday Foundation (OPS, FO), RSC BMCS Researcher Mobility Fellowship (MV), the Swedish Cancer Society (24 3848 Pj to PS, 24–0829-PT FMH, CAN2021/1490 to TH), a Novo Nordisk Pioneer Innovator Grant (NNF23OC0085944 MM), a Novo Nordisk Project Grant (NNF23OC0084420 VML), the Bengt Lundqvists Minne (JH), the Swedish Research Council (2021–02801, 2023–03015, 2024–03401 to VML, 021–06383 to TH, 2022–03681 to PS), European Research Council Proof of Concept grant SPHERO-NASH [Agreement no: 101123215] to VML, The Swedish Childhood Cancer Fund (PR2021-0030 OW), the Åke Wiberg Foundation (M23-0043 MM), Karolinska Institutet Research Foundation Grant (2022–01776 MM), Grant PID2020-115978GB-I00 (MdV) funded by MCIN/AEI/10.13039/501100011033. This project has received funding from the Innovative Medicines Initiative 2 Joint Undertaking (JU) under grant agreement No. s (MM, EJH, EW, IA, OG, KCL, AMK, VML). The JU receives support from the European Union's Horizon 2020 research and innovation programme and EFPIA and Ontario Institute for Cancer Research, Royal Institution for the Advancement of Learning McGill University, Kungliga Tekniska Högskolan, and Diamond Light Source Limited. This communication reflects the views of the authors, and the JU is not liable for any use that may be made of the information contained herein.

Conflict of Interests

VML is co-founder, CEO and shareholder of HepaPredict AB, as well as co-founder and shareholder of Shanghai Hepo Biotechnology Ltd. The other authors declare no competing interests.

Data Availability Statement

The data that support the findings of this study are available in the Supporting Information of this article.

Keywords: Base excision repair · DNA glycosylase · DNA repair · OGG1 · Organocatalytic switches

[1] R. Wang, W. Hao, L. Pan, I. Boldogh, X. Ba, *Cell. Mol. Life Sci.* **2018**, *75*, 3741.
[2] K. D. Jacob, N. Noren Hooten, T. Tadokoro, A. Lohani, J. Barnes, M. K. Evans, *F.Radic Biol. Med.* **2013**, *63*, 115.
[3] S. Oka, J. Leon, K. Sakumi, N. Abolhassani, Z. Sheng, D. Tsuchimoto, F. M. LaFerla, Y. Nakabeppu, *Sci. Rep.* **2021**, *11*, 5819.
[4] S. S. B. Komakula, J. Tumova, D. Kumaraswamy, N. Burchat, V. Vartanian, H. Ye, A. Dobrzyn, R. S. Lloyd, H. Sampath, *Sci. Rep.* **2018**, *8*, 14886.
[5] S. S. B. Komakula, B. Blaze, H. Ye, A. Dobrzyn, H. Sampath, *Int. J. Mol. Sci.* **2021**, *22*, 1152.
[6] B. A. Baptiste, S. R. Katchur, E. M. Fivenson, D. L. Croteau, W. L. Rumsey, V. A. Bohr, *Free Radic. Biol. Med.* **2018**, *124*, 149.
[7] T. Visnes, A. Cázares-Körner, W. Hao, O. Wallner, G. Masuyer, O. Loseva, O. Mortusewicz, E. Wiita, A. Sarno, A. Manoilov, J. Astorga-Wells, A.-S. Jemth, L. Pan, K. Sanjiv, S. Karsten, C. Gokturk, M. Grube, E. J. Homan, B. M. F. Hanna, C. B. J. Paulin, T. Pham, A. Rasti, U. W. Berglund, C. von Nicolai, C. Benitez-Buelga, T. Koolmeister, D. Ivanic, P. Iliev, M. Scobie, H. E. Krokan, et al., *Science* **2018**, *362*, 834.
[8] G. Gentric, V. Maillet, V. Paradis, D. Couton, A. L'Hermitte, G. Panasyuk, B. Fromenty, S. Celton-Morizur, C. Desdouets, *J. Clin. Invest.* **2015**, *125*, 981.
[9] J. C. Fromme, S. D. Bruner, W. Yang, M. Karplus, G. L. Verdine, *Nat. Struct. Mol. Biol.* **2003**, *10*, 204.
[10] E. C. Hank, N. D. D'Arcy-Evans, E. R. Scaletti, C. Benitez-Buelga, O. Wallner, F. Ortis, K. Zhou, L. Meng, P. Calvo, I. Almlöf, E. Wiita, S.

Kosenina, A. Krämer, M. Long, A.-S. Jemth, H. Dawson, J. Stewart, A. Dickey, M. E. Astorga, M. Varga, E. J. Homan, M. Scobie, S. Knapp, M. de Vega, L. Sastre, P. Stenmark, T. Helleday, M. Michel, *ChemRxiv* **2023**, 10.26434/chemrxiv-2023-70gws-v4.

[11] C. Benitéz-Buelga, T. Helleday, M. Michel, *Clin. Transl. Med.* **2022**, *12*, e1035.

[12] S. Youhanna, A. M. Kemas, S. C. Wright, Y. Zhong, B. Klumpp, K. Klein, A. Motso, M. Michel, N. Ziegler, M. Shang, P. Sabatier, A. Kannt, H. Sheng, N. Oliva-Vilarnau, F. A. Büttner, B. Seashore-Ludlow, J. Schreiner, M. Windbergs, M. Cornillet, N. K. Björkström, A. J. Hülsmeier, T. Hornemann, J. V. Olsen, Y. Wang, R. Gramignoli, M. Sundström, V. M. Lauschke, *Adv. Sci.* **2024**, *12*, 2407572.

[13] M. Michel, C. Benítez-Buelga, P. A. Calvo, B. M. F. Hanna, O. Mortusewicz, G. Masuyer, J. Davies, O. Wallner, K. Sanjiv, J. J. Albers, S. Castañeda-Zegarra, A.-S. Jemth, T. Visnes, A. Sastre-Perona, A. N. Danda, E. J. Homan, K. Marimuthu, Z. Zhenjun, C. N. Chi, A. Sarno, E. Wiita, C. von Nicolai, A. J. Komor, V. Rajagopal, S. Müller, E. C. Hank, M. Varga, E. R. Scaletti, M. Pandey, S. Karsten, et al., *Science* **2022**, *376*, 1471.

[14] M. Michel, T. Visnes, E. J. Homan, B. Seashore-Ludlow, M. Hedenström, E. Wiita, K. Vallin, C. B. J. Paulin, J. Zhang, O. Wallner, M. Scobie, A. Schmidt, A. Jenmalm-Jensen, U. W. Berglund, T. Helleday, *ACS Omega* **2019**, *4*, 11642.

[15] O. Wallner, A. Cázares-Körner, E. R. Scaletti, G. Masuyer, T. Bekkhus, T. Visnes, K. Mamonov, F. Ortis, T. Lundbäck, M. Volkova, T. Koolmeister, E. Wiita, O. Loseva, M. Pandey, E. Homan, C. Benítez-Buelga, J. Davies, M. Scobie, U. W. Berglund, C. Kalderén, P. Stenmark, T. Helleday, M. Michel, *ChemMedChem* **2022**, *18*, e202200310..

[16] J. C. Shelley, A. Cholleti, L. L. Frye, J. R. Greenwood, M. R. Timlin, M. Uchimaya, *J. Comput. Aided Mol. Des.* **2007**, *21*, 681.

[17] S. Müller, S. Ackloo, A. A. Chawaf, B. Al-Lazikani, A. Antolin, J. B. Baell, H. Beck, S. Beedie, U. A. K. Betz, G. A. Bezerra, P. E. Brennan, D. Brown, P. J. Brown, A. N. Bullock, A. J. Carter, A. Chaikuad, M. Chaineau, A. Ciulli, I. Collins, J. Dreher, D. Drewry, K. Edfeldt, A. M. Edwards, U. Egner, S. V. Frye, S. M. Fuchs, M. D. Hall, I. V. Hartung, A. Hillisch, S. H. Hitchcock, et al., *RSC Med. Chem.* **2022**, *13*, 13.

[18] O. D'Augustin, V. Gaudon, C. Siberchicot, R. Smith, C. Chapuis, J. Depagne, X. Veaute, D. Busso, A.-M. Di Guilmi, B. Castaing, J. P. Radicella, A. Campalans, S. Huet, *Nucleic Acids Res.* **2023**, *51*, 4942.

[19] M. Ren, F. Gut, Y. Fan, J. Ma, X. Shan, A. Yikilmazsoy, M. Likhodeeva, K.-P. Hopfner, C. Zhou, *Nat. Commun.* **2024**, *15*, 9407.

[20] M. Noureddin, A. Vipani, C. Bresee, T. Todo, I. K. Kim, N. Alkhouri, V. W. Setiawan, T. Tran, W. S. Ayoub, S. C. Lu, A. S. Klein, V. Sundaram, N. N. Nissen, *Am. J. Gastroenterol.* **2018**, *113*, 1649.

[21] M. Stepanova, K. Kabbara, D. Mohess, M. Verma, A. Roche-Green, S. AlQahtani, J. Ong, P. Burra, Z. M. Younossi, *Hepatol. Commun.* **2022**, *6*, 1506.

Manuscript received: January 29, 2025
Revised manuscript received: April 15, 2025
Version of record online: ■■, ■■

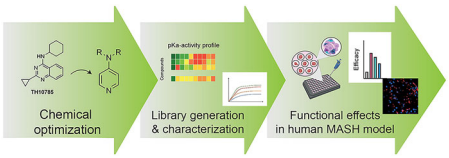

Organocatalytic switches are small molecules that combine active site affinity and a nitrogen-centered base for catalysis, effectively removing the rate-determining step of the OGG1 biochemical cascade. Here, we identify a minimal structure and modulate the active nitrogen pK_a, enabling the catalysis of ultrafast AP site incisions in a range of pH environments. Importantly, improved compounds exhibit potent anti-fibrotic effects in a patient-derived model of MASH.

M. Kehler, K. Zhou, A. M. Kemas, A. del Prado, E. S. Hutchinson, E. H. Nairn, M. Varga, Y. Plattner, Y. Zhong, O. Purewal-Sidhu, J. Haslam, E. Wiita, H. Gildie, K. Singerova, Z. Szaruga, I. Almlöf, F. M. Hormann, K.-C. Liu, O. Wallner, F. Ortis, E. J. Homan, O. Gileadi, S. G. Rudd, P. Stenmark, M. de Vega, T. Helleday, N. D. D'Arcy-Evans, V. M. Lauschke, M. Michel

1 – 10

Organocatalytic Switches of DNA Glycosylase OGG1 Catalyze a Highly Efficient AP-Lyase Function